
Superior generalization of smaller models in the presence of significant label noise

Yihao Xue

Department of Computer Science
University of California
Los Angeles, CA 90095, USA
yihaoxue@g.ucla.edu

Kyle Whitecross

Department of Computer Science
University of California
Los Angeles, CA 90095, USA
kswhitecross@g.ucla.edu

Baharan Mirzsoleiman

Department of Computer Science
University of California
Los Angeles, CA 90095, USA
baharan@cs.ucla.edu

Abstract

The benefits of over-parameterization in achieving superior generalization performance have been shown in several recent studies, justifying the trend of using larger models in practice. In the context of robust learning however, the effect of neural network size has not been well studied. In this work, we find that in the presence of a substantial fraction of mislabeled examples, increasing the network size beyond some point can be harmful. In particular, the originally monotonic or ‘double descent’ test loss curve (w.r.t. network width) turns into a U-shaped or a double U-shaped curve when label noise increases, suggesting that the best generalization is achieved by some model with intermediate size. We observe that when network size is controlled by density through random pruning, similar test loss behaviour is observed. We also take a closer look into both phenomenon through bias-variance decomposition and theoretically characterize how label noise shapes the variance term. Similar behavior of the test loss can be observed even when state-of-the-art robust methods are applied, indicating that limiting the network size could further boost existing methods. Finally, we empirically examine the effect of network size on the smoothness of learned functions, and find that the originally negative correlation between size and smoothness is flipped by label noise.

1 Introduction

The ever-increasing size of modern datasets allows large and overparameterized neural networks to achieve unprecedented success. The classical bias-variance tradeoff suggests that increasing the model size beyond some sweet spot will result in overfitting and negatively affect generalization performance. However, it has been widely observed that for overparameterized neural networks, increasing model size only improves generalization [38, 44, 6, 23]. Double descent [6, 44], proposed as a remedy for the conflicting views in classical and modern machine learning, breaks the test loss curve into two regimes: the classical/underparameterized regime where the loss exhibits U-shaped behavior, and the modern/overparameterized regime where the loss monotonically decreases. The two regimes are separated by the *interpolation threshold*.

As datasets grow larger, maintaining their quality becomes prohibitively expensive. In particular, the commonly used crowd-sourcing and automatic-labeling techniques introduce a lot of mislabeled

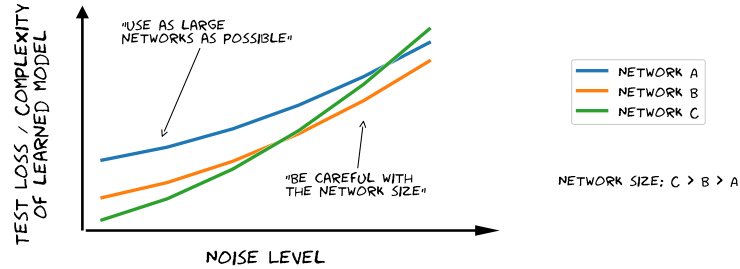


Figure 1: Label noise can flip the effect of network size on the test loss the complexity/smoothness of the learned function. See plots generated from real data in Appendix B

examples in big datasets. Over-parameterized networks have the capacity to memorize any (even random) labeling of the training data [55], hence a significant fraction of noisy labels drastically degrades their generalization performance. As machine learning is increasingly applied to high-risk and sensitive applications, it is necessary to ensure the robustness of the models deployed in the real world. Due to its importance, dealing with significant levels of noisy labels, e.g. 60%-80% symmetric noise on CIFAR10 and 40% noise on CIFAR100, is the main focus of all the recent studies on robust training against noisy labels [cite a lot of works]. This setting is particularly important as it represents the real-world scenarios in which the noise level is not as high, but the noise distribution is more complex than the synthetic symmetric or asymmetric noise. However, the effect of model size on generalization performance of models trained with significant levels of noisy labels has not been studied.

In this work, we thoroughly study the effect of neural network size on generalization in the presence of label noise and make the following observations/contributions:

- As we increase the noise level, the curve of the test loss w.r.t. network width transitions from the well known double-descent curve into a double U-shaped curve.
- Interestingly, when the network size is beyond optimal, even randomly pruning parameters at initialization can improve generalization.
- For both of the above results, we start with empirical observations and corroborate them with theoretical analysis on random feature ridge regression.
- We show that the above phenomena can be observed even when state-of-the-art robust methods (particularly DivideMix [28] and ELR [29]) are applied.
- We take a closer look into the smoothness of the learned functions and find that significant label noise can flip the originally negative correlation between size and complexity.

Overall our work reveals that the effect of network size on generalization can be flipped by label noise, as illustrated in Figure 1. Our results provide useful suggestions for practitioners on how to build more robust neural network architectures, and present broader challenges to designing robust learning methods.

2 Related Work

Generalization and overfitting of neural networks The traditional views on generalization have been renewed by recent counter-intuitive findings. On one hand, several recent studies have shown that contradictory to the classical bias-variance trade-off, increasing the size of overparameterized neural networks only improves generalization [38, 44, 6, 23], concluding that overfitting may not hurt generalization [22, 5]. Furthermore, it has been observed that small label noise does not change this behavior [54, 35]. It is also known that SGD biases towards simpler functions which generalize better, [7, 19, 22, 31] and a larger model architecture gives SGD more functions to select from. On the other hand, one may naturally expect the opposite. Since under large noise, gradient descent may be more affected by the noisy part of the data (theoretical evidence can be found in [9]), larger models may be more susceptible to overfitting.

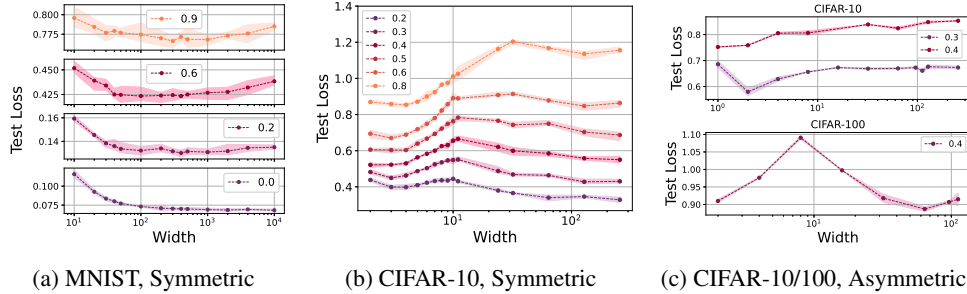


Figure 2: Under small noise, the test loss curve can either be monotonic (e.g., zero noise on MNIST) or the well-known double descent (e.g., 20%-50% noise on CIFAR-10). When the noise is large enough, the test loss will increase with the width after some point (20%-90% symmetric noise on MNIST, 60%-80% symmetric noise on CIFAR-10, 40% asymmetric noise on CIFAR-10/100).

Role of noise in double descent The role of label noise in double descent has been discussed in recent literature [35, 1, 12], while the focus is mainly on the effect of label noise on the peak at the interpolation threshold. The experimental studies carried out by [35] contain some experiments under 10-20% label noise showing that the risk is always monotonically decreasing after the peak, indicating that larger neural networks can make better prediction, even with a perfect fit on noisy training data. In this work we extend the experiments to higher noise levels and corroborate the new findings with theoretical analysis.

Neural network pruning before training. While in this work we simply use network pruning as a way to control the network size, we note that pruning before training has been an active research topic since the establishment of Lottery Ticket Hypothesis [13]. Works in this field mainly focus on extracting a sparse subnetwork from a dense neural network to alleviate training cost [26, 48, 51]. Our finding opens new doors to extending this technique to learning with label noise and provides an optimistic prediction of its success: an appropriate pruning ratio significantly improves the robustness of neural networks and even boosts the performance of SOTA robust learning methods.

Robust training against noisy labels. Methods for robust learning from noisy labels are mainly focused on estimating the noise transition matrix [15, 40], designing robust loss functions [14, 49, 52, 58], correcting noisy labels [32, 41, 47, 28], using explicit regularization techniques [8, 56, 57, 29], and selecting or reweighting training examples [10, 17, 21, 33, 42, 52, 34]. These efforts focus on developing algorithms to improve robustness. Recently [27] showed that choosing the right architecture leads to predictive representations even when the model is trained with label noise. Nonetheless, in most tasks the type of the architecture is predefined, so the remaining question is *what network size should we use*, which we address in this paper. The theory part in [27] considered the effect of *architecture alignment* on the *predictive power*, where *architecture alignment* is defined in terms of the sample complexity required to learn the target function and *predictive power* is defined as the performance of a linear probe trained on hidden features (outputs of hidden layers) with clean labels. This does not help us answer the above question because (1) the relationship between sample complexity and size remains unclear for modern neural networks. Recent studies even suggest that sample complexity and size are independent [16], and (2) as mentioned in [27] the *predictive power* can be high even when the test performance is bad and therefore it is not directly related to generalization.

3 Label Noise Can Flip the Effect of Network Size on Generalization

3.1 Larger Width Can Hurt Generalization

We start by empirically investigating the test loss of models of increasing width under various levels of label noise. We train a two-layer ReLU network on MNIST [25] and ResNet34 [18] on CIFAR-10 [24] (see Appendix A for details). The width of the two-layer network is controlled by the number of hidden neurons and the width of ResNet is controlled by the number of convolutional layer filters. We consider two types of noise in the experiments: symmetric noise, where the labels of certain

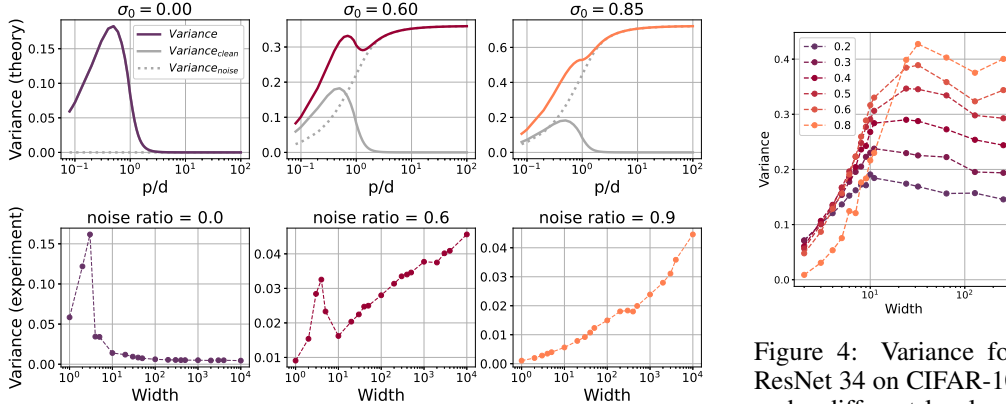


Figure 3: Top: the curve plotted based on the expressions in Theorem 1 and Appendix C.2. Bottom: variance for a two-layer ReLU network on trained on MNIST with symmetric noise. We attribute the second ascent to $\mathbf{Variance}_{\text{noise}}$ which increases with both the width and noise level.

Figure 4: Variance for ResNet 34 on CIFAR-10 under different levels of symmetric noise. For noise levels 0.6 and 0.8, the second ascent occurs at width 128.

fraction of training examples are randomly flipped, and asymmetric noise, where wrong labels are generated in a class-dependent way to mimic real-world noise. See the details in Appendix A.1.

Results are presented in Figure 2. Under zero or small label noise, test loss can either be monotonically decreasing (0% noise in 2a) or double descent (20% to 50% noise in 2b). As the noise level is increased, there will eventually be a width beyond which the test loss monotonically increases. For MNIST with 20% to 60% label noise (Figure 2a), the curves of test loss are U-shaped. For CIFAR-10 with 60% to 80% noise (Figure 2b), the curves of test loss are double U-shaped, and the optimal width is even in the under parameterized regime at the bottom of the first U-shaped curve.

We note that the phenomenon *larger models hurt* can be observed under smaller noise levels when the noise is asymmetric, as is shown in Figure 2c. This is not surprising since asymmetric noise is considered as a stronger type of noise than symmetric noise. Since real-world label noise is usually class-dependent or even instance-dependent, such behavior can occur under moderate noise level and therefore attentions should be paid in practice.

3.1.1 The Second Ascent in Variance Caused by Label Noise

To understand how label noise changes the effect of width on test loss, we look at the bias-variance decomposition: $\mathbf{Loss} = \mathbf{Bias}^2 + \mathbf{Variance}$. Despite the difference in the philosophies of decomposing the variance term, recent works [12, 54, 1] agree on the shapes of bias and total variance: the bias is monotonically decreasing and the variance is unimodal, which is confirmed by the experimental results on various network architectures, datasets and loss functions [54]. Here, we first empirically show that under large label noise, the variance manifests as unimodal followed by a *second ascent*. Then we explain this observation by providing a theoretical example where the variance can be decomposed into a noise-independent unimodal term and a monotonically increasing term that scales as the noise level.

Empirical observations. To empirically measure the bias-variance decomposition of the loss, we apply the unbiased estimator proposed in [54] to calculate the unbiased empirical variance of the network output across splits of training set. To do so, we randomly split the training set for each model into N subsets ($N = 6$ for MNIST and $N = 5$ for CIFAR-10), train a copy of the model for each subset and take the average test loss. In both settings we use MSE loss because the bias-variance decomposition is only well defined for MSE (see equation 1) which can be empirically measured by an unbiased estimator [54]. We see in Figures 3 (bottom row) and 4 that as the label noise increases, the end of the originally unimodal variance curve eventually goes up.

Theoretical results. Now we provide a theoretical analysis on a two-layer linear network to explain why the second ascent occurs. Suppose we have a training dataset (\mathbf{X}, \mathbf{y}) where $\mathbf{X} =$

$[\mathbf{x}_1, \mathbf{x}_2, \dots, \mathbf{x}_n]$ and $\mathbf{y} = [y_1, y_2, \dots, y_n]^\top$, with $\mathbf{x}_i \in \mathbb{R}^d$ and $y_i \in \mathbb{R}$ are feature vector and label point data point i . We assume each \mathbf{x}_i is independently drawn from a Gaussian distribution $\mathcal{N}(0, \mathbf{I}_d/d)$ and labels are generated by $y_i = \mathbf{x}_i^\top \boldsymbol{\theta} + \epsilon_i$ where $\boldsymbol{\theta} \in \mathbb{R}^d$ with entries independently drawn from $N(0, 1)$ and $\epsilon_i \in \mathbb{R}$ is the label noise drawn from $N(0, \sigma^2)$ for each \mathbf{x}_i . The learned function is given by random feature ridge regression. Specifically, we learn a two-layer linear network where the first layer $\mathbf{W} \in \mathbb{R}^{p \times d}$ has each entry randomly drawn from $\mathcal{N}(0, 1/d)$ and the second layer is given by

$$\hat{\boldsymbol{\beta}} = \arg \min_{\boldsymbol{\beta} \in \mathbb{R}^p} \|(\mathbf{W}\mathbf{X})^\top \boldsymbol{\beta} - \mathbf{y}\|^2 + \lambda \|\boldsymbol{\beta}\|^2 = (\mathbf{W}\mathbf{X}\mathbf{X}^\top \mathbf{W}^\top + \lambda \mathbf{I})^{-1} \mathbf{W}\mathbf{X}(\mathbf{X}^\top \boldsymbol{\theta} + \boldsymbol{\epsilon}),$$

where $\boldsymbol{\epsilon} = [\epsilon_1, \epsilon_2, \dots, \epsilon_n]^\top$. Given a clean test example (\mathbf{x}, y) where $\mathbf{x} \sim \mathcal{N}(0, \mathbf{I}_d/d)$ and $y = \mathbf{x}^\top \boldsymbol{\theta}$, the prediction of the learned model is given by $f(\mathbf{x}) = (\mathbf{W}\mathbf{x})^\top \hat{\boldsymbol{\beta}}$. The expected test loss can then be written as

$$\begin{aligned} \text{Risk} &= \mathbb{E}_{\boldsymbol{\theta}} \mathbb{E}_{\mathbf{x}} \mathbb{E}_{\mathbf{X}, \mathbf{W}, \boldsymbol{\epsilon}} (f(\mathbf{x}) - y)^2 = \underbrace{\mathbb{E}_{\boldsymbol{\theta}} \mathbb{E}_{\mathbf{x}} (\mathbb{E}_{\mathbf{X}, \mathbf{W}, \boldsymbol{\epsilon}} f(\mathbf{x}) - y)^2}_{\text{Bias}^2} + \underbrace{\mathbb{E}_{\boldsymbol{\theta}} \mathbb{E}_{\mathbf{x}} \mathbb{V}_{\mathbf{X}, \mathbf{W}, \boldsymbol{\epsilon}} f(\mathbf{x})}_{\text{Variance}} \quad (1) \\ &= \underbrace{\frac{1}{d} \|\mathbb{E}_{\mathbf{X}, \mathbf{W}} \mathbf{B} - \mathbf{I}\|_F^2}_{\text{Bias}^2} + \underbrace{\frac{1}{d} \mathbb{E}_{\mathbf{X}, \mathbf{W}} \|\mathbf{B} - \mathbb{E}_{\mathbf{X}, \mathbf{W}} \mathbf{B}\|_F^2}_{\text{Variance}_{\text{clean}}} + \underbrace{\frac{\sigma^2}{d} \mathbb{E}_{\mathbf{X}, \mathbf{W}} \|\mathbf{A}\|_F^2}_{\text{Variance}_{\text{noise}}}, \end{aligned}$$

where $\mathbf{A} := \mathbf{W}^\top (\mathbf{W}\mathbf{X}\mathbf{X}^\top \mathbf{W}^\top + \lambda \mathbf{I})^{-1} \mathbf{W}\mathbf{X}$ and $\mathbf{B} := \mathbf{A}\mathbf{X}^\top$. See the derivation in Appendix C.1. Recently, [54] analyzed Bias^2 and $\text{Variance}_{\text{clean}}$, i.e., the bias-variance decomposition without label noise, in the asymptotic scaling limit where n , d and p all tend to infinity with $\frac{n}{d} = \infty$ and $\frac{p}{d} = \gamma$. The exact expressions of Bias^2 and $\text{Variance}_{\text{clean}}$ showing that Bias^2 is monotonic and $\text{Variance}_{\text{clean}}$ is unimodal are given in the Appendix C.2. In Theorem 1 below, we extend their result by presenting the closed-form expression of $\text{Variance}_{\text{noise}}$ in the same asymptotic regime.

Theorem 1. *For a 2-layer linear network with p hidden neurons and a random first layer, consider learning the second layer by ridge regression with parameter λ on n training examples with feature dimension d and label noise with variance σ , let $\lambda = \frac{n}{d} \lambda_0$ and $\sigma^2 = \frac{n}{d} \sigma_0^2$ for some fixed λ_0 and σ_0^2 . The asymptotic expression (where $n, d, p \rightarrow \infty$ with $\frac{n}{d} = \infty$ and $\frac{p}{d} = \gamma$) of $\text{Variance}_{\text{noise}}$ is given by*

$$\text{Variance}_{\text{noise}} = \frac{\sigma_0^2}{2} \left(\gamma + 2\lambda_0 + 1 - \frac{\gamma^2 + (3\lambda_0 - 2)\gamma + 2\lambda_0^2 + 3\lambda_0 + 1}{\sqrt{\gamma^2 + (2\lambda_0 - 2)\gamma + \lambda_0^2 + 2\lambda_0 + 1}} \right).$$

We plot the expressions in the top row of Figure 3 with $\lambda_0 = 0.1$. The dashed gray line shows $\text{Variance}_{\text{noise}}$ monotonically increases with γ . The solid gray line shows $\text{Variance}_{\text{clean}}$ based on the expression in [54] and the blue line shows the sum, i.e., Variance (the total variance). We see that the shape of Variance perfectly matches that of the variance measured in experiments (Figure 3, bottom row).

Our analysis provides a straightforward explanation: there is a term $\text{Variance}_{\text{noise}}$ in the total variance that increases with both width and label noise. When label noise is large enough so that $\text{Variance}_{\text{noise}}$ reaches the scale comparable to $\text{Variance}_{\text{clean}}$, the second ascent occurs (Figure 3, middle column). In this case the risk can be either U-shaped (c.f. 20% or 60% label noise in Figure 2) or double U-shaped (c.f. 60% or 80% label noise in Figure 2), depending on the relative scales of bias and $\text{Variance}_{\text{clean}}$. Moreover, under extreme noise where $\text{Variance}_{\text{noise}}$ dominates the variance (Figure 3, right column), the double-descent (or sometimes monotonic) curve degenerates to a U-shaped curve as in classical bias-variance tradeoff where both bias and variance are monotonic.

3.2 Smaller Density Can Help Generalization

As we discussed in Section 3.1, increasing width will eventually hurt the performance in presence of large label noise. Motivated by this finding, we study another natural approach for controlling the network size: pruning network connections before training, which reduces the number of trainable parameters without removing neurons. While one can easily change the width of ResNet by adjusting the number of channels in each block, for more complex models that are heavily engineered, e.g., the Inception-ResNet family [45] (which we experiment with in Section 5), there is no straightforward way to do so without significant change to the architecture. Here, specifying the network by pruning a fraction of weights is of interest as a more practical way to control the network size.

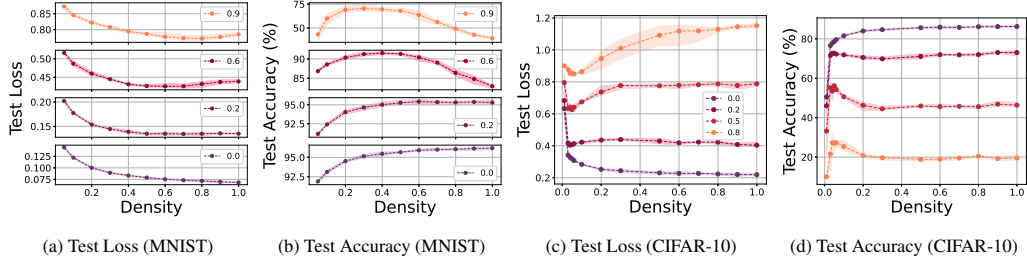


Figure 5: Test loss and accuracy of models with different densities on MNIST and CIFAR-10 under symmetric noise.

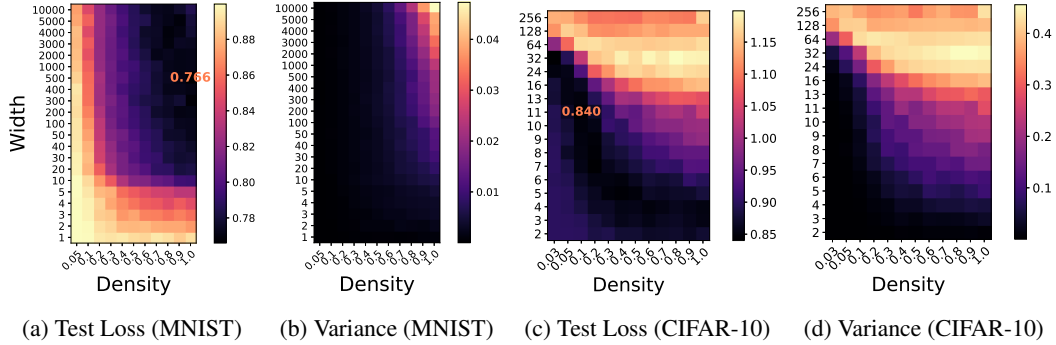


Figure 6: Risk (a)(c) and variance (b)(d) with varied widths and densities measured in experiments on MNIST and CIFAR-10. For MNIST the lowest loss is achieved width 500 and density 1 (though the highest test accuracy is achieved by a small density, see Appendix B). For CIFAR-10 the lowest loss is achieved by width 11 with density 0.1. In both settings, the variance increases with both density and width after some point.

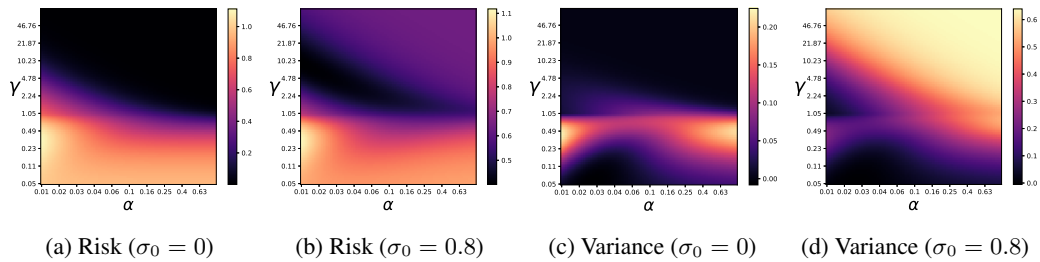


Figure 7: Risk (a)(b) and variance (c)(d) with varied widths and densities given by theorem 2. Notably, the variance under zero noise (c) is non-monotonic w.r.t. either width or density and therefore differs from that in classical bias-variance tradeoff.

Empirical observations. We conduct experiments on MNIST, CIFAR-10, under the same settings as in section 3.1 with symmetric noise. After initialization, we randomly prune a certain fraction of weights and keep them at 0 throughout the training. Figure 5 shows how the performance changes with density under different noise levels. Under zero or small label noise, random pruning only hurts the performance. While for larger label noise, e.g., 60% on MNIST, 50% and 80% on CIFAR-10, the test loss first decreases and then increases, with the increase of density.

Since the effect of density can also be dependent on the width of the architecture, to see the whole picture of how these two quantities jointly affect the test loss, we further conduct experiments on 90% corrupted MNIST and 80% corrupted CIFAR-10 with varying both width and density. The results are given in Figures 6a and 6c with the annotated number in red showing which model achieves the lowest test loss. As we can see, the best models are not the largest ones at the top right corner, and there is an increasing trend in the loss towards the top-right corner. Notably, for CIFAR-10 the model with lowest loss has width 11 and density 0.1, which outperforms any

full-density model with smaller width. This suggests that pruning as a more fine-grained capacity control can find the optimal size that can not be achieved by merely tuning the width. For MNIST, while the lowest loss is achieved by an unpruned model, as we show in Appendix B the model with highest test accuracy has a density of 0.3.

We explore the variance of the test loss in Figures 6b and 6d. The key observation is that in both figures there is an increasing trend towards the top-right corner, though for CIFAR-10 the behavior is non-monotonic and more complicated. Note that the variance curve for 0.8 noise ratio in Figure 4 is exactly the rightmost column in Figure 6d. As we discussed in Section 3.1.1 there is a second ascent in the variance. Hence, we should expect higher variance for widths larger than 256 with density 1. We also show the monotonically decreasing (along both axes) bias in Appendix B.

Theoretical results. We now corroborate our empirical results with a theoretical analysis which characterizes the effects of both width and density. The random feature regression setting of Theorem 1 where the first layer of the network is random and the second layer is trained can not distinguish pruning from reducing width because the parameter of the second layer is a vector. We instead consider a three-layer linear network where the first layer is the same as in Theorem 1 whose output yields random features, the second layer is pruned and trained, and the last layer is also random. Formally, the function represented by the network is $f(\mathbf{x}) = ((\mathbf{V} \odot \mathbf{M})\mathbf{W}\mathbf{x})^\top \boldsymbol{\mu}$. \mathbf{W} and \mathbf{X} are the same as in Theorem 1. $\mathbf{V} \in \mathbb{R}^{q \times p}$, $\mathbf{M} \in \{0, 1\}^{q \times p}$ with entries independently drawn from $Bernoulli(\alpha)$ where $\alpha \in [0, 1]$ is the density. $\boldsymbol{\mu} \in \mathbb{R}^q$ with entries independently drawn from $\mathcal{N}(0, 1/q)$ (we set the variance to $1/q$ to cancel the effect of q thus the network size is only controlled by p and α so that we can plot the risk in a 2-D plane; of course we have other choices, e.g. set it to $1/d$ and let $q = p$, see those variants in Appendix C.5). We show that, in the above setting, in terms of the risk and its decomposition, it is equivalent to replacing the λ_0 in Theorem 1 with λ_0/α . See the proof in Appendix C.4.

Theorem 2. *For a 3-layer linear network with p first-layer hidden neurons and both the first and last layers random, consider learning the second layer by ridge regression with random masks drawn from $Bernoulli(\alpha)$. Let λ , n and σ be the ridge regression parameter, number of training examples and noise level, respectively. Let $\lambda = \frac{n}{d}\lambda_0$ and $\sigma^2 = \frac{n}{d}\sigma_0^2$ for some fixed λ_0 and σ_0^2 . The asymptotic expressions (where $n, d, p \rightarrow \infty$ with $\frac{n}{d} = \infty$ and $\frac{p}{d} = \gamma$) of **Risk**, **Bias**², **Variance**_{clean} and **Variance**_{noise} are given by their counterparts in the setting of Theorem 1 with λ_0 substituted with λ_0/α .*

Figure 7 shows the plots for risk and variance under different noise levels given by Theorem 2 with $\lambda_0 = 0.05$. See in Appendix C.6 for the plots for the bias and the decomposition of variance. Under zero noise, the risk monotonically decreases along both axes (Figure 7a), and the variance is unimodal along y-axis, manifests more complicated behavior along x-axis, and decreases along both axes once width is sufficiently large (Figure 7c). When noise is large, we see that the trend in both the risk and variance match the empirical results in Figure 6: the lowest risk is given by models with intermediate width and density (and the optimal density under given width decreases as the width increases) and the variance increases towards the top-right corner.

Pruning vs. regularization. One may notice that Theorem 2 implies that pruning is equivalent to increasing the strength of l_2 regularization by the inverse factor. Such equivalence may not hold for neural networks considering the non-linearity and the optimization process. Our empirical results show that pruning can achieve a lower loss/higher accuracy than that of tuning l_2 regularization and we defer the plots and discussion to Appendix B.

3.3 Effect of Width and Density for Models Trained with Robust Methods

The above experiments are all conducted with standard training procedure. However, in noisy settings robust methods are usually applied to achieve reasonable test performance. One may ask whether the above situation can be turned around by these methods, since they are specially designed to counter the effect of label noise. To answer this question we experiment with two state-of-the-art robust methods: ELR [29] and DivideMix[28]. ELR leverages the early learning phenomenon where the network fits clean examples first and then wrongly-labeled examples. It mitigates overfitting by regularizing the loss with a term that encourages the alignment between the model’s prediction and the running average of the predictions in previous rounds. DivideMix dynamically discards labels that are highly likely to be noisy and trains the model in a semi-supervised

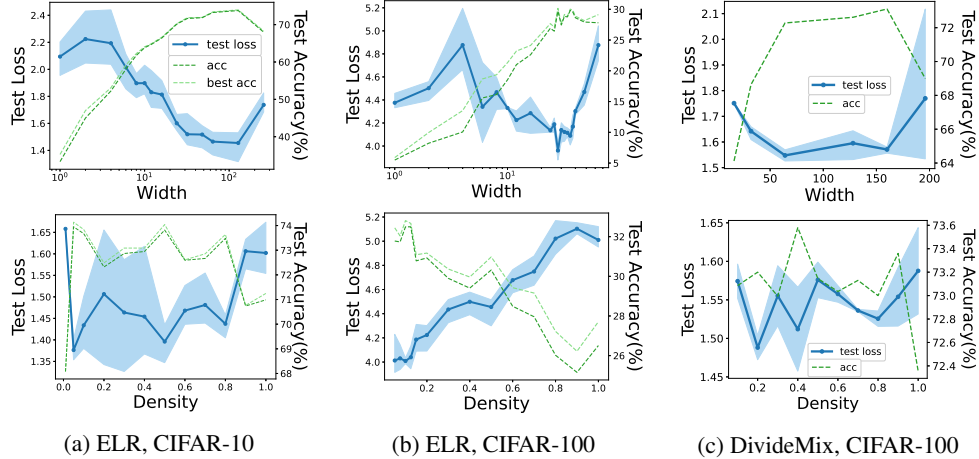


Figure 8: (a,b) ELR on CIFAR-10 and CIFAR-100 under 80% symmetric noise. ‘best acc’ refers to the highest test accuracy observed during training, which is usually reported in robust method papers. In pruning experiments we use width 128 for CIFAR-10 and width 64 for CIFAR-100. (c) DivideMix on CIFAR-100 with 60% symmetric noise. DivideMix uses two networks to perform sample selection, so we change the width of both.

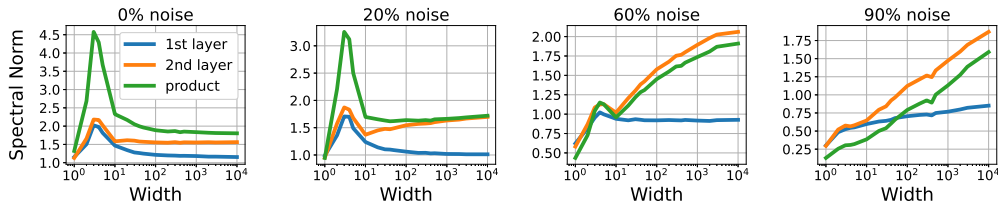


Figure 9: Spectral norm of a two-layer ReLU network trained on MNIST. The product of spectral norms of layers is known to be an upper bound for the Lipschitz constant. Interestingly, the shape of the product is similar to that of the variance in Figure 3, which can be explained by the intimate relation between model complexity and variance.

manner. We train ResNet34 on CIFAR-10 and CIFAR-100 with these methods using the same training setup as reported in the original papers [29, 28]. See in Appendix A for more details.

Figure 8 presents the cases where size controlling is still important for models trained with these methods. The optimal size we observed for ELR is 128 on CIFAR-10, and 28 on CIFAR-100. This contradicts the prevailing intuition that one should always use larger models for more complex tasks. Actually the same amount of label noise can be more harmful on more complex datasets (e.g., per-class label noise on CIFAR-100 is $10\times$ that on CIFAR-10), and the weakness of a too rich hypothesis class is more pronounced. For networks with width 128 on CIFAR-10 and width 64 on CIFAR-100, pruning to extreme density greatly improves the performance. Notably, pruning out 90% of the parameters improves the test accuracy from 27.73% (29.87% reported in [29]) to 32.92%, indicating that even random pruning can be used to boost robust methods to achieve SOTA performance. For DivideMix, the test performance becomes worse when we increase the width beyond 160 or increase the density beyond 0.8.

Similar phenomenon can also be observed under moderate noise levels. Figure 15 shows the results of ELR on CIFAR-10 with 30% asymmetric noise and on CIFAR-100 with 40 symmetric noise.

4 A Closer Look into the Smoothness of Learned Functions

A core component in (theoretical or empirical) analysis of generalization is the notion of a complexity measure; a quantity that monotonically relates to some aspect of generalization. More specifically, a lower complexity should often imply a smaller generalization gap. A complexity

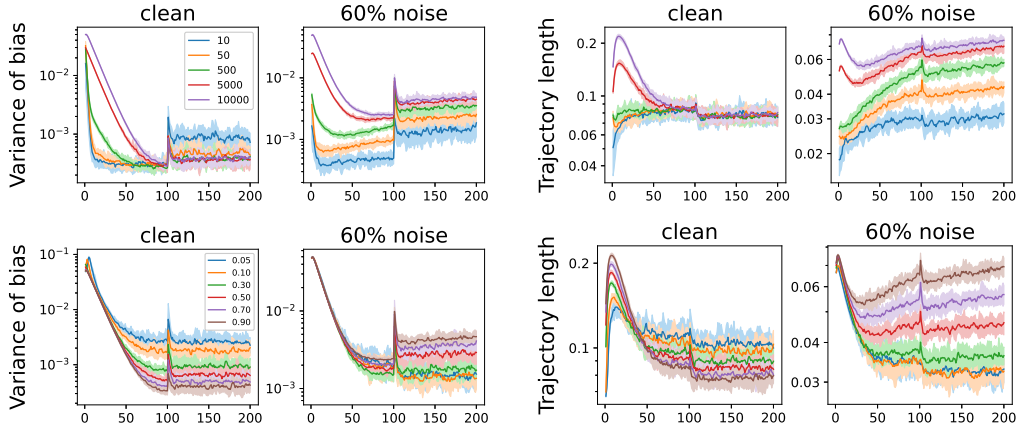


Figure 10: Trajectory length and variance of the first layer bias in the two-layer ReLU network with varied width (top) and density (bottom). We see that the effects of network size on both quantities are flipped by label noise.

measure may depend on the properties of the trained model, optimizer, and possibly training data. Theoretically motivated complexity measures such as norm [4], sharpness [37, 11], etc., as well as empirically motivated ones are often featured as the major components of generalization bounds.

In this section, we look into Lipschitz constant, a quantity of special importance for its theoretical [53, 36] and empirical [39] correlation with generalization. Since exactly computing the Lipschitz constants of neural networks is known to be NP-hard [50], we instead consider (1) the spectral norm, known as an upper bound for the Lipschitz constant [46], and (2) the trajectory of the first layer bias [30], which sheds light on both training dynamics and local Lipschitz constant. We observe on a two-layer neural network (trained on MNIST with the same set up as in Section 3) that these two quantities both decrease with the network size on clean dataset and increase with the network size under label noise. Figure 9 shows that the end of spectral norm curve goes up as we increase the noise level. In Figure 10 we see that on the clean dataset the algorithm learns functions with potentially larger local Lipschitz at the end of training (indicated by larger variance of first-layer bias and trajectory length), while for 60% it's the other way around. This finding suggests that the originally negative correlation between size and complexity/smoothness can be flipped by label noise.

5 Experiments on Real-world Noisy Data

Next we examine our findings in a real-world setting: training a heavily engineered architecture on a dataset containing real-world noise results from human mislabeling. In particular, here we train InceptionResNet-v2 [45] on Red Stanford Cars [20] whose images are annotated using the Google Cloud labeling service. The details of the dataset and training setup are in Appendix A. The noise level is approximately 70.5%. Due to the intricate nature of such architecture, we control the network size through pruning. For each density, we repeat the experiment 4 times and take the average of the performance. We also repeat the experiment with ELR. The results presented in Figure 11 confirm the benefit of the size controlling in realistic scenarios. In particular, both with and without ELR, the best accuracy occurs at a density less than 100%, substantiating our findings that model size control is important to achieve the best performance.

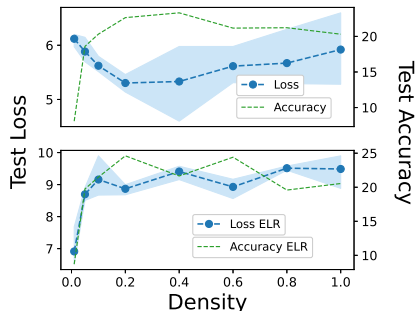


Figure 11: The performance of InceptionResNet-v2 trained on Red Stanford Cars.

6 Discussion and Future Work

Despite the recent counter-intuitive findings on the generalization of neural networks, our work suggests that the classical wisdom of capacity control is still useful in the context of learning with label noise. Meanwhile, we also expect that stronger robust methods can be designed (e.g., by enforcing the simplicity/smoothness of learned functions) to fully unleash the expressive power of larger neural networks.

We have observed that network size control through random pruning can benefit robustness a lot. It is natural to ask: can we do better than random? And if so, what makes the optimal subnetwork special? Answering these questions may make it possible to derive more powerful robust learning techniques and a deeper insight into the role of network architecture.

To help practitioners efficiently find the optimal network size, it will be important to extend the empirical scaling laws (functional approximations of the test loss in terms of certain quantities such as width and pruning level), e.g., neural scaling laws [23, 2] and the scaling law for pruning [43] to noisy settings. And these new laws should be able to characterize the non-monotonic behavior of the test loss under label noise.

We only consider label noise generated randomly or introduced by human labeling. It will be valuable to investigate whether large models are more vulnerable in the presence of adversarial noise or even attacks.

References

- [1] Ben Adlam and Jeffrey Pennington. Understanding double descent requires a fine-grained bias-variance decomposition. *Advances in neural information processing systems*, 33:11022–11032, 2020.
- [2] Yasaman Bahri, Ethan Dyer, Jared Kaplan, Jaehoon Lee, and Utkarsh Sharma. Explaining neural scaling laws. *arXiv preprint arXiv:2102.06701*, 2021.
- [3] Zhidong Bai and Jack W Silverstein. *Spectral analysis of large dimensional random matrices*, volume 20. Springer, 2010.
- [4] Peter L Bartlett, Dylan J Foster, and Matus J Telgarsky. Spectrally-normalized margin bounds for neural networks. *Advances in neural information processing systems*, 30, 2017.
- [5] Peter L Bartlett, Philip M Long, Gábor Lugosi, and Alexander Tsigler. Benign overfitting in linear regression. *Proceedings of the National Academy of Sciences*, 117(48):30063–30070, 2020.
- [6] Mikhail Belkin, Daniel Hsu, Siyuan Ma, and Soumik Mandal. Reconciling modern machine-learning practice and the classical bias–variance trade-off. *Proceedings of the National Academy of Sciences*, 116(32):15849–15854, 2019.
- [7] Alon Brutzkus, Amir Globerson, Eran Malach, and Shai Shalev-Shwartz. Sgd learns over-parameterized networks that provably generalize on linearly separable data. *arXiv preprint arXiv:1710.10174*, 2017.
- [8] Kaidi Cao, Yining Chen, Junwei Lu, Nikos Arechiga, Adrien Gaidon, and Tengyu Ma. Heteroskedastic and imbalanced deep learning with adaptive regularization. *arXiv preprint arXiv:2006.15766*, 2020.
- [9] Yuan Cao, Zixiang Chen, Mikhail Belkin, and Quanquan Gu. Benign overfitting in two-layer convolutional neural networks. *arXiv preprint arXiv:2202.06526*, 2022.
- [10] Pengfei Chen, Ben Ben Liao, Guangyong Chen, and Shengyu Zhang. Understanding and utilizing deep neural networks trained with noisy labels. In *International Conference on Machine Learning*, pages 1062–1070, 2019.
- [11] Gintare Karolina Dziugaite and Daniel M Roy. Computing nonvacuous generalization bounds for deep (stochastic) neural networks with many more parameters than training data. *arXiv preprint arXiv:1703.11008*, 2017.

- [12] Stéphane d’Ascoli, Maria Refinetti, Giulio Biroli, and Florent Krzakala. Double trouble in double descent: Bias and variance (s) in the lazy regime. In *International Conference on Machine Learning*, pages 2280–2290. PMLR, 2020.
- [13] Jonathan Frankle and Michael Carbin. The lottery ticket hypothesis: Finding sparse, trainable neural networks. *arXiv preprint arXiv:1803.03635*, 2018.
- [14] Aritra Ghosh, Himanshu Kumar, and PS Sastry. Robust loss functions under label noise for deep neural networks. In *Thirty-First AAAI Conference on Artificial Intelligence*, 2017.
- [15] Jacob Goldberger and Ehud Ben-Reuven. Training deep neural-networks using a noise adaptation layer. 2016.
- [16] Noah Golowich, Alexander Rakhlin, and Ohad Shamir. Size-independent sample complexity of neural networks. In *Conference On Learning Theory*, pages 297–299. PMLR, 2018.
- [17] Bo Han, Quanming Yao, Xingrui Yu, Gang Niu, Miao Xu, Weihua Hu, Ivor Tsang, and Masashi Sugiyama. Co-teaching: Robust training of deep neural networks with extremely noisy labels. In *Advances in neural information processing systems*, pages 8527–8537, 2018.
- [18] Kaiming He, Xiangyu Zhang, Shaoqing Ren, and Jian Sun. Deep residual learning for image recognition. In *Proceedings of the IEEE conference on computer vision and pattern recognition*, pages 770–778, 2016.
- [19] Ziwei Ji and Matus Telgarsky. The implicit bias of gradient descent on nonseparable data. In *Conference on Learning Theory*, pages 1772–1798. PMLR, 2019.
- [20] Lu Jiang, Di Huang, Mason Liu, and Weilong Yang. Beyond synthetic noise: Deep learning on controlled noisy labels. In *International Conference on Machine Learning*, pages 4804–4815. PMLR, 2020.
- [21] Lu Jiang, Zhengyuan Zhou, Thomas Leung, Li-Jia Li, and Li Fei-Fei. Mentornet: Learning data-driven curriculum for very deep neural networks on corrupted labels. In *International Conference on Machine Learning*, pages 2309–2318, 2018.
- [22] Dimitris Kalimeris, Gal Kaplun, Preetum Nakkiran, Benjamin Edelman, Tristan Yang, Boaz Barak, and Haofeng Zhang. Sgd on neural networks learns functions of increasing complexity. *Advances in neural information processing systems*, 32, 2019.
- [23] Jared Kaplan, Sam McCandlish, Tom Henighan, Tom B Brown, Benjamin Chess, Rewon Child, Scott Gray, Alec Radford, Jeffrey Wu, and Dario Amodei. Scaling laws for neural language models. *arXiv preprint arXiv:2001.08361*, 2020.
- [24] Alex Krizhevsky, Geoffrey Hinton, et al. Learning multiple layers of features from tiny images. 2009.
- [25] Yann LeCun. The mnist database of handwritten digits. <http://yann.lecun.com/exdb/mnist/>, 1998.
- [26] Namhoon Lee, Thalaiyasingam Ajanthan, and Philip HS Torr. Snip: Single-shot network pruning based on connection sensitivity. *arXiv preprint arXiv:1810.02340*, 2018.
- [27] Jingling Li, Mozhi Zhang, Keyulu Xu, John Dickerson, and Jimmy Ba. How does a neural network’s architecture impact its robustness to noisy labels? *Advances in Neural Information Processing Systems*, 34, 2021.
- [28] Junnan Li, Richard Socher, and Steven CH Hoi. Dividemix: Learning with noisy labels as semi-supervised learning. *arXiv preprint arXiv:2002.07394*, 2020.
- [29] Sheng Liu, Jonathan Niles-Weed, Narges Razavian, and Carlos Fernandez-Granda. Early-learning regularization prevents memorization of noisy labels. *Advances in neural information processing systems*, 33:20331–20342, 2020.
- [30] Andreas Loukas, Marinos Pooitis, and Stefanie Jegelka. What training reveals about neural network complexity. *Advances in Neural Information Processing Systems*, 34, 2021.

- [31] Kaifeng Lyu, Zhiyuan Li, Runzhe Wang, and Sanjeev Arora. Gradient descent on two-layer nets: Margin maximization and simplicity bias. *Advances in Neural Information Processing Systems*, 34, 2021.
- [32] Xingjun Ma, Yisen Wang, Michael E Houle, Shuo Zhou, Sarah Erfani, Shutao Xia, Sudanthi Wijewickrema, and James Bailey. Dimensionality-driven learning with noisy labels. In *International Conference on Machine Learning*, pages 3355–3364, 2018.
- [33] Eran Malach and Shai Shalev-Shwartz. Decoupling" when to update" from" how to update". In *Advances in Neural Information Processing Systems*, pages 960–970, 2017.
- [34] Baharan Mirzasoleiman, Kaidi Cao, and Jure Leskovec. Coresets for robust training of deep neural networks against noisy labels. *Advances in Neural Information Processing Systems*, 33, 2020.
- [35] Preetum Nakkiran, Gal Kaplun, Yamini Bansal, Tristan Yang, Boaz Barak, and Ilya Sutskever. Deep double descent: Where bigger models and more data hurt. *Journal of Statistical Mechanics: Theory and Experiment*, 2021(12):124003, 2021.
- [36] Behnam Neyshabur, Srinadh Bhojanapalli, David McAllester, and Nati Srebro. Exploring generalization in deep learning. *Advances in neural information processing systems*, 30, 2017.
- [37] Behnam Neyshabur, Srinadh Bhojanapalli, and Nathan Srebro. A pac-bayesian approach to spectrally-normalized margin bounds for neural networks. *arXiv preprint arXiv:1707.09564*, 2017.
- [38] Behnam Neyshabur, Ryota Tomioka, and Nathan Srebro. In search of the real inductive bias: On the role of implicit regularization in deep learning. *arXiv preprint arXiv:1412.6614*, 2014.
- [39] Roman Novak, Yasaman Bahri, Daniel A Abolafia, Jeffrey Pennington, and Jascha Sohl-Dickstein. Sensitivity and generalization in neural networks: an empirical study. *arXiv preprint arXiv:1802.08760*, 2018.
- [40] Giorgio Patrini, Alessandro Rozza, Aditya Krishna Menon, Richard Nock, and Lizhen Qu. Making deep neural networks robust to label noise: A loss correction approach. In *Proceedings of the IEEE Conference on Computer Vision and Pattern Recognition*, pages 1944–1952, 2017.
- [41] Scott Reed, Honglak Lee, Dragomir Anguelov, Christian Szegedy, Dumitru Erhan, and Andrew Rabinovich. Training deep neural networks on noisy labels with bootstrapping. *arXiv preprint arXiv:1412.6596*, 2014.
- [42] Mengye Ren, Wenyuan Zeng, Bin Yang, and Raquel Urtasun. Learning to reweight examples for robust deep learning. In *International Conference on Machine Learning*, pages 4334–4343, 2018.
- [43] Jonathan S Rosenfeld, Jonathan Frankle, Michael Carbin, and Nir Shavit. On the predictability of pruning across scales. In *International Conference on Machine Learning*, pages 9075–9083. PMLR, 2021.
- [44] Stefano Spigler, Mario Geiger, Stéphane d’Ascoli, Levent Sagun, Giulio Biroli, and Matthieu Wyart. A jamming transition from under-to over-parametrization affects generalization in deep learning. *Journal of Physics A: Mathematical and Theoretical*, 52(47):474001, 2019.
- [45] Christian Szegedy, Sergey Ioffe, Vincent Vanhoucke, and Alexander A Alemi. Inception-v4, inception-resnet and the impact of residual connections on learning. In *Thirty-first AAAI conference on artificial intelligence*, 2017.
- [46] Christian Szegedy, Wojciech Zaremba, Ilya Sutskever, Joan Bruna, Dumitru Erhan, Ian Goodfellow, and Rob Fergus. Intriguing properties of neural networks. *arXiv preprint arXiv:1312.6199*, 2013.
- [47] Daiki Tanaka, Daiki Ikami, Toshihiko Yamasaki, and Kiyoharu Aizawa. Joint optimization framework for learning with noisy labels. In *Proceedings of the IEEE Conference on Computer Vision and Pattern Recognition*, pages 5552–5560, 2018.

- [48] Hidenori Tanaka, Daniel Kunin, Daniel L Yamins, and Surya Ganguli. Pruning neural networks without any data by iteratively conserving synaptic flow. *Advances in Neural Information Processing Systems*, 33:6377–6389, 2020.
- [49] Brendan Van Rooyen, Aditya Menon, and Robert C Williamson. Learning with symmetric label noise: The importance of being unhinged. In *Advances in Neural Information Processing Systems*, pages 10–18, 2015.
- [50] Aladin Virmaux and Kevin Scaman. Lipschitz regularity of deep neural networks: analysis and efficient estimation. *Advances in Neural Information Processing Systems*, 31, 2018.
- [51] Chaoqi Wang, Guodong Zhang, and Roger Grosse. Picking winning tickets before training by preserving gradient flow. *arXiv preprint arXiv:2002.07376*, 2020.
- [52] Xinshao Wang, Yang Hua, Elyor Kodirov, and Neil M Robertson. Imae for noise-robust learning: Mean absolute error does not treat examples equally and gradient magnitude’s variance matters. *arXiv preprint arXiv:1903.12141*, 2019.
- [53] Huan Xu and Shie Mannor. Robustness and generalization. *Machine learning*, 86(3):391–423, 2012.
- [54] Zitong Yang, Yaodong Yu, Chong You, Jacob Steinhardt, and Yi Ma. Rethinking bias-variance trade-off for generalization of neural networks. In *International Conference on Machine Learning*, pages 10767–10777. PMLR, 2020.
- [55] Chiyuan Zhang, Samy Bengio, Moritz Hardt, Benjamin Recht, and Oriol Vinyals. Understanding deep learning requires rethinking generalization. *arXiv preprint arXiv:1611.03530*, 2016.
- [56] Han Zhang, Honglak Lee, Sercan Arik, Tomas Pfister, and Zizhao Zhang. Distilling effective supervision from severe label noise. 2020.
- [57] Hongyi Zhang, Moustapha Cisse, Yann N Dauphin, and David Lopez-Paz. mixup: Beyond empirical risk minimization. *arXiv preprint arXiv:1710.09412*, 2017.
- [58] Zhilu Zhang and Mert Sabuncu. Generalized cross entropy loss for training deep neural networks with noisy labels. In *Advances in neural information processing systems*, pages 8778–8788, 2018.

Checklist

1. For all authors...
 - (a) Do the main claims made in the abstract and introduction accurately reflect the paper’s contributions and scope? [Yes]
 - (b) Did you describe the limitations of your work? [Yes]
 - (c) Did you discuss any potential negative societal impacts of your work? [N/A]
 - (d) Have you read the ethics review guidelines and ensured that your paper conforms to them? [Yes]
2. If you are including theoretical results...
 - (a) Did you state the full set of assumptions of all theoretical results? [Yes]
 - (b) Did you include complete proofs of all theoretical results? [Yes]
3. If you ran experiments...
 - (a) Did you include the code, data, and instructions needed to reproduce the main experimental results (either in the supplemental material or as a URL)? [Yes]
 - (b) Did you specify all the training details (e.g., data splits, hyperparameters, how they were chosen)? [Yes]
 - (c) Did you report error bars (e.g., with respect to the random seed after running experiments multiple times)? [Yes]
 - (d) Did you include the total amount of compute and the type of resources used (e.g., type of GPUs, internal cluster, or cloud provider)? [Yes]

4. If you are using existing assets (e.g., code, data, models) or curating/releasing new assets...
 - (a) If your work uses existing assets, did you cite the creators? [Yes]
 - (b) Did you mention the license of the assets? [N/A]
 - (c) Did you include any new assets either in the supplemental material or as a URL? [Yes]

 - (d) Did you discuss whether and how consent was obtained from people whose data you're using/curating? [N/A]
 - (e) Did you discuss whether the data you are using/curating contains personally identifiable information or offensive content? [N/A]
5. If you used crowdsourcing or conducted research with human subjects...
 - (a) Did you include the full text of instructions given to participants and screenshots, if applicable? [N/A]
 - (b) Did you describe any potential participant risks, with links to Institutional Review Board (IRB) approvals, if applicable? [N/A]
 - (c) Did you include the estimated hourly wage paid to participants and the total amount spent on participant compensation? [N/A]

A Details of Experiments

All experiments are implemented using PyTorch. We use four Nvidia A40 to run the experiments.

A.1 Noise Generation

Symmetric noise We first select a fraction of training examples then randomly shuffle their labels. For example, on CIFAR-10, if the noise level is 50%, the resulting fraction of mislabeled examples is expected to be around $0.9 \times 50\% = 45\%$.

Asymmetric noise The noise is class-dependent. We follow the scheme proposed in [40] which is also widely used in robust method papers (e.g., ELR [29] and DivideMix [28]). For CIFAR-10, labels are randomly flipped according to the following map: TRUCK→AUTOMOBILE, BIRD→AIRPLANE, DEER→HORSE, CAT→DOG, DOG→CAT. For CIFAR-100, since the 100 classes are grouped into 20 superclasses, e.g. AQUATIC MAMMALS contains BEAVER, DOLPHIN, OTTER, SEAL and WHALE, we flip labels of each class into the next one circularly within super-classes. For both datasets, the fraction of mislabeled examples in the training set is the noise level.

A.2 Basic Experiments

To apply the estimator provided in [54], each time we train a model, we split the training set into N subsets ($N = 6$ for MNIST and $N = 5$ for CIFAR-10), train a copy of the model for each subset and take the average test loss. The variance is estimated by calculating the variance of the network output across splits of training set. And the squared bias is estimated by subtracting the variance from the average loss. The training setup is given by the following.

MNIST We train a two-layer ReLU network for 200 epochs using SGD with batch size 128, momentum 0.9, initial learning rate 0.1, a weight decay of 5×10^{-4} , a learning rate decay of 0.1 at epoch 100.

CIFAR-10 We train ResNet34 for 1000 epochs using SGD with batch size 128, momentum 0.9, initial learning rate 0.1, weight decay of 5×10^{-4} , learning rate decay of 0.1 every 400 epochs. For width w , there are $w, 2w, 4w, 8w$ filters in each layer of the four Residual Blocks, respectively.

A.3 Experiments with Robust Methods

For both ELR and DivideMix we use the same setup in the original papers. [29, 28].

ELR We train ResNet-34 using SGD with momentum 0.9, a weight decay of 0.001, and a batch size of 128. The network is trained for 120 epochs on CIFAR-10 and 150 epochs on CIFAR-100. The learning rate is 0.02 at initialization, and decayed by a factor of 100 at epochs 40 and 80 for CIFAR-10 and at epochs 80 and 120 for CIFAR-100. We use 0.7 for the temporal ensembling parameter, and 3 for the ELR regularization coefficient.

DivideMix We train ResNet-34 for 200 epochs using SGD with batch size 64, momentum 0.9, initial learning rate 0.02, a weight decay of 5×10^{-4} , and a learning rate decay of 0.1 at epoch 150. We use 150 for the unsupervised loss weight.

A.4 Experiments with Real-world Noise

We train InceptionResNet-v2[45] on Red Stanford Car[20]. There are 10 different noise levels for Red Stanford Car and we choose 80%. In particular, 6469 out of the 8144 images in the dataset are annotated incorrectly by human annotators, which can only be downloaded from the provided URLs¹. However, 590 of the images cannot be downloaded and among the downloaded JPG files 1871 are corrupted and unopenable, hence we end up with 1675 clean examples and 4008 noisy examples, i.e., the actual noise level is 70.53%.

¹See their webpage for details <https://google.github.io/controlled-noisy-web-labels/download.html>

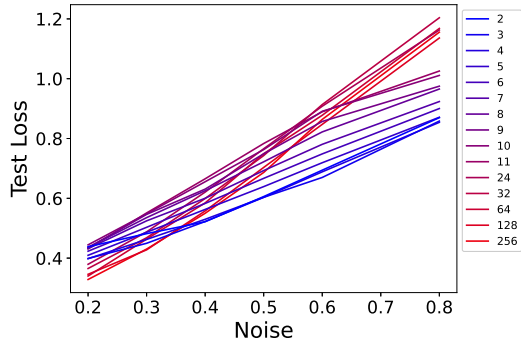
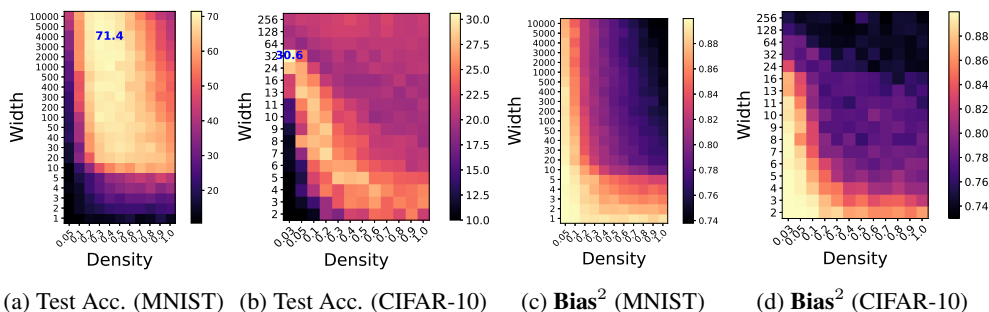


Figure 12: Test Loss w.r.t. noise level for varied width, i.e., we replot Figure 2b but switch the x-axis and the legend.



(a) Test Acc. (MNIST) (b) Test Acc. (CIFAR-10) (c) Bias^2 (MNIST) (d) Bias^2 (CIFAR-10)

Figure 13: Heatmaps of test accuracy and bias of ResNet34 trained on CIFAR-10.

We train the network for 160 epochs with an initial learning rate of 0.1, and a weight decay of 1×10^{-5} using SGD and momentum of 0.9 with a batch size of 32. We anneal the learning rate by a factor of 10 at epochs 80 and 120, respectively.

B Additional Empirical Results

Test loss w.r.t. noise Figure 12 is a counterpart of Figure 1 plotted with results on CIFAR-10. The colors show the widths. We see that the noise hurts larger models more, and as a result, when the noise reaches certain point the effect of width on test loss is flipped.

Additional results for section 3.2 Figure 13 show the heatmaps of test accuracy and bias. The bias of models with varied width and density is shown in Figures 13c and 13d. In both settings the bias monotonically decreases w.r.t. both width or density. We also present the heatmaps of test accuracy in 13a and 13b. On MNIST, the highest accuracy is achieved by width 4000 and density 0.4. On CIFAR-10 it is achieved by width 32 and density 0.03.

Pruning vs. l_2 regularization In the setting of Theorem 2, we show that pruning the network is equivalent to increasing the strength of l_2 regularization. To see whether this applies to more complex settings, we train ResNet34 on CIFAR-10 with 50% symmetric noise with varied weight decay and network density. Results are shown in Figure 14. Three observations are made here,

- In both cases the shape of the curve is similar (e.g., both loss curves are U-shaped), implying that increasing weight decay and reducing density have a similar effect on the loss.
- The relation between density and weight decay is not exactly the inverse relationship as is in Theorem 2 (otherwise the two curves would overlap). This can be a result of the complicated effect of nonlinearities in deep neural networks.
- We can see that pruning can achieve a lower loss/higher accuracy than that of l_2 regularization. We conjecture this is because pruning also significantly changes the loss landscape

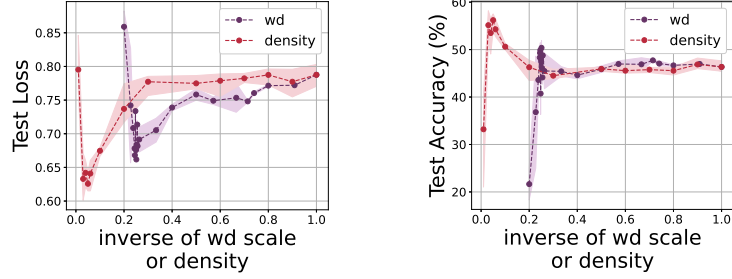


Figure 14: Comparing effects of the strength l_2 regularization (weight decay) and network density. We use CIFAR-10 with 50% symmetric noise as our dataset. For weight decay experiments, the density is fixed to 1. For density experiments, weight decay is fixed to 0.0005. The x-axis is the inverse of the scale-up of weight decay, i.e., the current weight decay divided by 0.0005, for the weight decay curve (purple), and the density for the density curve (red).

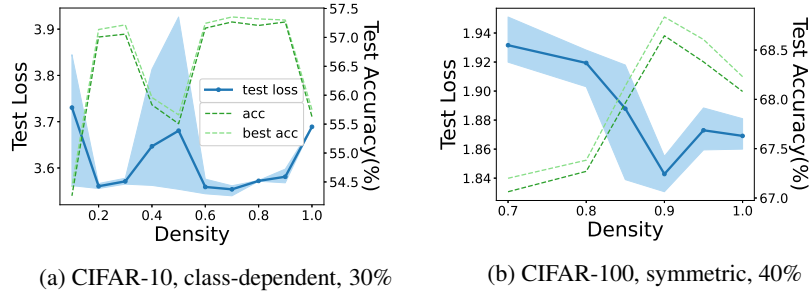


Figure 15: Experiments on CIFAR with varied network density when the model is trained by ELR.

and makes optimization harder, as a result SGD may not be able to find the global minima, but instead gets stuck at a local minima which somehow generalizes better. In other words, for modern neural networks, pruning may have some benefit beyond capacity control.

More experiments with ELR Fig 15 shows that increasing density eventually hurts the performance under 30% asymmetric noise on CIFAR10, and 40% symmetric noise on CIFAR100 when the model is trained with ELR.

C Theoretical Results

Notations: We use bold-faced letter for matrix and vectors. The training dataset is denoted by (\mathbf{X}, \mathbf{y}) where $\mathbf{X} = [\mathbf{x}_1, \mathbf{x}_2, \dots, \mathbf{x}_n]$ and $\mathbf{y} = [y_1, y_2, \dots, y_n]^\top$, with $\mathbf{x}_i \in \mathbb{R}^d$ and $y_i \in \mathbb{R}$ are feature vector and label point data point i . We assume each \mathbf{x}_i is independently drawn from a Gaussian distribution $\mathcal{N}(0, \mathbf{I}_d/d)$ and labels are generated by $y_i = \mathbf{x}_i^\top \boldsymbol{\theta} + \epsilon_i$ where $\boldsymbol{\theta} \in \mathbb{R}^d$ with entries independently drawn from $N(0, 1)$ and $\epsilon_i \in \mathbb{R}$ is the label noise drawn from $N(0, \sigma^2)$ for each \mathbf{x}_i . And we assume each test example (\mathbf{x}, y) is clean, i.e., $y = \mathbf{x}^\top \boldsymbol{\theta}$.

C.1 Bias-Variance Decomposition of the MSE Loss in Section 3.1

Here we show the derivation of Equation 1.

$$\begin{aligned}
\mathbf{Bias}^2 &= \mathbb{E}_\theta \mathbb{E}_x (\mathbb{E}_{\mathbf{X}, \mathbf{W}, \epsilon} f(\mathbf{x}) - y)^2 \\
&= \mathbb{E}_\theta \mathbb{E}_x (\mathbb{E}_{\mathbf{X}, \mathbf{W}, \epsilon} ((\mathbf{W}\mathbf{x})^\top \hat{\beta}) - y)^2 \\
&= \mathbb{E}_\theta \mathbb{E}_x [\mathbf{x}^\top (\mathbb{E}_{\mathbf{X}, \mathbf{W}, \epsilon} (\mathbf{B}\boldsymbol{\theta} + \mathbf{A}\epsilon) - \boldsymbol{\theta})]^2 \\
&= \mathbb{E}_\theta \mathbb{E}_x \text{Tr}[(\mathbb{E}_{\mathbf{X}, \mathbf{W}, \epsilon} (\mathbf{B}\boldsymbol{\theta}) - \boldsymbol{\theta})^\top \mathbf{x}\mathbf{x}^\top (\mathbb{E}_{\mathbf{X}, \mathbf{W}, \epsilon} (\mathbf{B}\boldsymbol{\theta}) - \boldsymbol{\theta})] \\
&= \mathbb{E}_\theta \text{Tr}[(\mathbb{E}_{\mathbf{X}, \mathbf{W}, \epsilon} (\mathbf{B}\boldsymbol{\theta}) - \boldsymbol{\theta})^\top \mathbb{E}_x (\mathbf{x}\mathbf{x}^\top) (\mathbb{E}_{\mathbf{X}, \mathbf{W}, \epsilon} (\mathbf{B}\boldsymbol{\theta}) - \boldsymbol{\theta})] \\
&= \frac{1}{d} \mathbb{E}_\theta \|\mathbb{E}_{\mathbf{X}, \mathbf{W}, \epsilon} (\mathbf{B}\boldsymbol{\theta}) - \boldsymbol{\theta}\|_F^2 \\
&= \frac{1}{d} \mathbb{E}_\theta \text{Tr}[(\mathbb{E}_{\mathbf{X}, \mathbf{W}} \mathbf{B} - \mathbf{I})\boldsymbol{\theta}\boldsymbol{\theta}^\top (\mathbb{E}_{\mathbf{X}, \mathbf{W}} \mathbf{B} - \mathbf{I})] \\
&= \frac{1}{d} \text{Tr}[(\mathbb{E}_{\mathbf{X}, \mathbf{W}} \mathbf{B} - \mathbf{I})\mathbb{E}_\theta (\boldsymbol{\theta}\boldsymbol{\theta}^\top) (\mathbb{E}_{\mathbf{X}, \mathbf{W}} \mathbf{B} - \mathbf{I})] \\
&= \frac{1}{d} \|\mathbb{E}_{\mathbf{X}, \mathbf{W}} \mathbf{B} - \mathbf{I}\|_F^2
\end{aligned}$$

$$\begin{aligned}
\mathbf{Variance} &= \mathbb{E}_\theta \mathbb{E}_x \mathbb{V}_{\mathbf{X}, \mathbf{W}, \epsilon} f(\mathbf{x}) \\
&= \mathbb{E}_\theta \mathbb{E}_x \mathbb{E}_{\mathbf{X}, \mathbf{W}, \epsilon} [\mathbf{x}^\top (\mathbf{B}\boldsymbol{\theta} + \mathbf{A}\epsilon) - \mathbb{E}_{\mathbf{X}, \mathbf{W}, \epsilon} \mathbf{x}^\top (\mathbf{B}\boldsymbol{\theta} + \mathbf{A}\epsilon)]^2 \\
&= \frac{1}{d} \mathbb{E}_\theta \mathbb{E}_{\mathbf{X}, \mathbf{W}, \epsilon} \|(\mathbf{B}\boldsymbol{\theta} + \mathbf{A}\epsilon) - \mathbb{E}_{\mathbf{X}, \mathbf{W}} \mathbf{B}\boldsymbol{\theta}\|_F^2 \\
&= \frac{1}{d} \mathbb{E}_\theta \mathbb{E}_{\mathbf{X}, \mathbf{W}, \epsilon} \|(\mathbf{B} - \mathbb{E}_{\mathbf{X}, \mathbf{W}} \mathbf{B})\boldsymbol{\theta} + \mathbf{A}\epsilon\|_F^2 \\
&= \frac{1}{d} \mathbb{E}_\theta \mathbb{E}_{\mathbf{X}, \mathbf{W}} \|(\mathbf{B} - \mathbb{E}_{\mathbf{X}, \mathbf{W}} \mathbf{B})\boldsymbol{\theta}\|_F^2 + \frac{1}{d} \mathbb{E}_{\mathbf{X}, \mathbf{W}, \epsilon} \|\mathbf{A}\epsilon\|_F^2 \\
&= \underbrace{\frac{1}{d} \mathbb{E}_{\mathbf{X}, \mathbf{W}} \|\mathbf{B} - \mathbb{E}_{\mathbf{X}, \mathbf{W}} \mathbf{B}\|_F^2}_{\mathbf{Variance}_{\text{clean}}} + \underbrace{\frac{\sigma^2}{d} \mathbb{E}_{\mathbf{X}, \mathbf{W}} \|\mathbf{A}\|_F^2}_{\mathbf{Variance}_{\text{noise}}}
\end{aligned}$$

C.2 Expressions of Bias and Variance_clean

[54] analyzed the bias-variance decomposition without considering label noise. Hence the variance in their analysis corresponds to $\mathbf{Variance}_{\text{clean}}$ in our analysis. We show their expressions below, based on which we plot the dashed curve in Figure 3 ($\mathbf{Variance}_{\text{clean}}$) and dashed gray in Figure 16 (\mathbf{Bias}^2).

$$\begin{aligned}
\mathbf{Bias}^2 &= \frac{1}{4} \Phi_3(\lambda_0, \gamma)^2 \\
\mathbf{Variance}_{\text{clean}} &= \begin{cases} \frac{\Phi_1(\lambda_0, \gamma)}{2\Phi_2(\lambda_0, \gamma)} - \frac{(1-\gamma)(1-2\gamma)}{2\gamma} - \frac{1}{4} \Phi_3(\lambda_0, \gamma)^2, & \gamma \leq 1, \\ \frac{\Phi_1(\lambda_0, 1/\gamma)}{2\Phi_2(\lambda_0, 1/\gamma)} - \frac{\gamma-1}{2} - \frac{1}{4} \Phi_3(\lambda_0, \gamma)^2, & \gamma > 1, \end{cases}
\end{aligned}$$

where

$$\begin{aligned}
\Phi_1(\lambda_0, \gamma) &= \lambda_0(\gamma + 1) + (\gamma - 1)^2, \\
\Phi_2(\lambda_0, \gamma) &= \sqrt{(\lambda_0 + 1)^2 + 2(\lambda_0 - 1)\gamma + \gamma^2}, \\
\Phi_3(\lambda_0, \gamma) &= \Phi_2(\lambda_0, \gamma) - \lambda_0 - \gamma + 1.
\end{aligned}$$

C.3 Proof of Theorem 1

Lemma 3. Define $\tilde{\mathbf{B}} = \mathbf{W}^\top (\mathbf{W}\mathbf{W}^\top + \lambda_0 \mathbf{I})^{-1} \mathbf{W}$. $\|\tilde{\mathbf{B}}\tilde{\mathbf{B}}^\top - \frac{n}{d} \mathbf{A}\mathbf{A}^\top\|_2 = 0$ almost surely, i.e., $\mathbb{P}(\|\tilde{\mathbf{B}}\tilde{\mathbf{B}}^\top - \frac{n}{d} \mathbf{A}\mathbf{A}^\top\|_2 \leq \epsilon) \geq 1 - \delta$ where ϵ and δ both tend to 0 under the asymptotics $n \rightarrow \infty$, $d \rightarrow \infty$ and $n/d \rightarrow \infty$.

Proof. Define

$$\begin{aligned}\Delta &:= \frac{d}{n} \mathbf{X} \mathbf{X}^\top - I, \\ \Psi &:= (\mathbf{W} \mathbf{W}^\top + \lambda_0 I)^{-1} \\ \Gamma &:= \left(\frac{d}{n} \mathbf{W} \mathbf{X} \mathbf{X}^\top \mathbf{W}^\top + \lambda_0 I \right)^{-1} \\ \Omega &:= \Gamma - \Psi.\end{aligned}$$

Then we have

$$\begin{aligned}\tilde{\mathbf{B}} \tilde{\mathbf{B}}^\top - \frac{n}{d} \mathbf{A} \mathbf{A}^\top &= \Omega \mathbf{W} \Delta \mathbf{W}^\top \Omega + \Psi \mathbf{W} \Delta \mathbf{W}^\top \Psi + \Omega \mathbf{W} \Delta \mathbf{W}^\top \Psi + \Psi \mathbf{W} \Delta \mathbf{W}^\top \Omega \\ &\quad + \Omega \mathbf{W} \mathbf{W}^\top \Omega + \Omega \mathbf{W} \mathbf{W}^\top \Psi + \Psi \mathbf{W} \mathbf{W}^\top \Omega.\end{aligned}$$

By triangle inequality and the sub-multiplicative property of spectral norm we have

$$\begin{aligned}\|\tilde{\mathbf{B}} \tilde{\mathbf{B}}^\top - \frac{n}{d} \mathbf{A} \mathbf{A}^\top\|_2 &\leq \|\mathbf{W}\|_2^2 \|\Omega\|_2^2 \|\Delta\|_2 + \|\mathbf{W}\|_2^2 \|\Psi\|_2^2 \|\Delta\|_2 + 2 \|\mathbf{W}\|_2^2 \|\Psi\|_2 \|\Omega\|_2 \|\Delta\|_2 \\ &\quad + \|\mathbf{W}\|_2^2 \|\Omega\|_2^2 + 2 \|\mathbf{W}\|_2^2 \|\Psi\|_2 \|\Omega\|_2\end{aligned}$$

It remains to show that with the asymptotic assumption $n/d \rightarrow \infty$, $\|\Omega\|_2 = 0$ and $\|\Delta\|_2 = 0$ almost surely, and $\|\mathbf{W}\|_2$ and $\|\Psi\|_2$ can be bounded from above [54]:

$$\begin{aligned}\mathbb{P}(\|\Delta\|_2 \leq 4\sqrt{\frac{d}{n}} + 4\frac{d}{n}) &\geq 1 - e^{-d/2} \\ \|\Omega\|_2 &\leq \|\Psi\|_2^2 \|\mathbf{W}\|_2^2 \|\Delta\|_2 + O(\|\Delta\|_2) \\ \|\mathbf{W}\|_2 &\stackrel{a.s.}{\leq} 1 + \sqrt{\eta} < \infty \\ \|\Psi\|_2 &\leq \frac{1}{\lambda_0} < \infty.\end{aligned}$$

Therefore we have $\|\tilde{\mathbf{B}} \tilde{\mathbf{B}}^\top - \frac{n}{d} \mathbf{A} \mathbf{A}^\top\|_2 = 0$ almost surely. \square

Corollary 4. $\frac{\sigma^2}{d} \|\mathbf{A}\|_F^2 = \frac{\sigma_0^2}{d} \|\tilde{\mathbf{B}}\|_F^2$ almost surely.

Proof. By lemma 3 we have

$$\begin{aligned}|\operatorname{Tr}(\frac{1}{n} \tilde{\mathbf{B}} \tilde{\mathbf{B}}^\top - \frac{1}{d} \mathbf{A} \mathbf{A}^\top)| &= \frac{1}{n} \operatorname{Tr}(\tilde{\mathbf{B}} \tilde{\mathbf{B}}^\top - \frac{n}{d} \mathbf{A} \mathbf{A}^\top) \\ &\leq \frac{d}{n} \|\tilde{\mathbf{B}} \tilde{\mathbf{B}}^\top - \frac{n}{d} \mathbf{A} \mathbf{A}^\top\|_2 \\ &= 0,\end{aligned}$$

which yields $\frac{1}{d} \|\mathbf{A}\|_F^2 = \frac{1}{n} \|\tilde{\mathbf{B}}\|_F^2$ and then $\frac{\sigma^2}{d} \|\mathbf{A}\|_F^2 = \frac{\sigma_0^2}{d} \|\tilde{\mathbf{B}}\|_F^2$. \square

Now it only remains to compute $\frac{1}{d} \|\tilde{\mathbf{B}}\|_F^2$. By Sherman–Morrison formula,

$$\tilde{\mathbf{B}} = I - (I + \frac{\alpha}{\eta} \mathbf{Q})^{-1},$$

where $\alpha = \lambda_0^{-1}$, $\mathbf{Q} = (d/p) \mathbf{W}^\top \mathbf{W}$ and $\eta = d/p = 1/\gamma$. Let $F^\mathbf{Q}$ be the empirical spectral distribution of \mathbf{Q} , i.e.,

$$F^\mathbf{Q}(x) = \frac{1}{d} \#\{j \leq d : \lambda_j \leq x\},$$

where $\#S$ denotes the cardinality of the set S and λ_j denotes the j -th eigenvalue of \mathbf{Q} . Then

$$\frac{\|\tilde{\mathbf{B}}\|_F^2}{d} = \int_{\mathbb{R}^+} \frac{(\frac{\alpha}{\eta} x)^2}{(1 + \frac{\alpha}{\eta} x)^2} dF^\mathbf{Q}(x).$$

By Marchenko-Pastur Law [3],

$$\begin{aligned}\frac{\|\tilde{\mathbf{B}}\|^2}{d} &= \frac{1}{2\pi} \int_{\eta_-}^{\eta_+} \frac{\sqrt{(\eta_+ - x)(x - \eta_-)} \left(\frac{\alpha}{\eta} x\right)^2}{\eta x \left(1 + \frac{\alpha}{\eta} x\right)^2} dx \\ &= \frac{1}{2\alpha} \left(\frac{-\alpha^2/\eta^2 - (3\alpha - 2\alpha^2)/\eta - \alpha^2 - 3\alpha - 2}{\sqrt{\alpha^2/\eta^2 + (2\alpha - 2\alpha^2)/\eta + \alpha^2 + 2\alpha + 1}} + \alpha/\eta + \alpha + 2 \right).\end{aligned}\quad (2)$$

Combining equation 2 and corollary 4 and substituting $\alpha = \lambda_0^{-1}$, $\eta = \gamma^{-1}$ into the result completes the proof.

C.4 Proof of Theorem 2

Define the following shorthand

$$\begin{aligned}\mathbf{F} &:= \mathbf{W}\mathbf{X} \\ \mathbf{D}_i &:= \text{diag}(\mathbf{M}_{i,1}, \mathbf{M}_{i,2}, \dots, \mathbf{M}_{i,p}) \\ \mu_i &:= i\text{-th entry of } \boldsymbol{\mu} \\ \mathbf{V}_i^\top &:= i\text{-th row of } \mathbf{V} \\ \boldsymbol{\Sigma} &:= \sum_{i=1}^q \mu_i^2 \mathbf{D}_i \\ \mathbf{H} &:= \mathbf{y}^\top \mathbf{F}^\top \boldsymbol{\Sigma} \mathbf{F} (\mathbf{F}^\top \boldsymbol{\Sigma} \mathbf{F} + \lambda \mathbf{I})^{-1}\end{aligned}$$

The parameter of the second layer is given by ridge regression:

$$\begin{aligned}\hat{\mathbf{V}} &= \arg \min_{\mathbf{V} \in \mathbb{R}^{q \times p}} \|((\mathbf{V} \odot \mathbf{M})\mathbf{W}\mathbf{X})^\top \boldsymbol{\mu} - \mathbf{y}\|_F^2 + \lambda \|\mathbf{V}\|_F^2 \\ &= \arg \min_{\mathbf{V} \in \mathbb{R}^{q \times p}} \left\| \sum_{i=1}^q \mu_i \mathbf{V}_i^\top \mathbf{D}_i \mathbf{F} - \mathbf{y}^\top \right\|_F^2 + \lambda \|\mathbf{V}\|_F^2.\end{aligned}$$

Solving the above yields

$$\hat{\mathbf{V}}_i^\top = \frac{1}{\lambda} (\mathbf{y}^\top - \mathbf{H}) \mathbf{F}^\top (\mu_i \mathbf{D}_i).$$

Given a clean test example (\mathbf{x}, \mathbf{y}) , the expression of the risk is

$$\begin{aligned}\mathbf{Risk} &= \mathbb{E} \left\| \sum_{i=1}^q \mu_i \hat{\mathbf{V}}_i^\top \mathbf{W}\mathbf{x} - \boldsymbol{\theta}^\top \mathbf{x} \right\|_F^2 \\ &= \mathbb{E} \left\| \frac{1}{\lambda} (\mathbf{y}^\top - \mathbf{H}) \mathbf{F}^\top \boldsymbol{\Sigma} \mathbf{W}\mathbf{x} - \boldsymbol{\theta}^\top \mathbf{x} \right\|_F^2 \\ &= \mathbb{E} \left\| \frac{1}{\lambda} (\mathbf{y}^\top - \mathbf{y}^\top \mathbf{F}^\top \boldsymbol{\Sigma} \mathbf{F} (\mathbf{F}^\top \boldsymbol{\Sigma} \mathbf{F} + \lambda \mathbf{I})^{-1}) \mathbf{F}^\top \boldsymbol{\Sigma} \mathbf{W}\mathbf{x} - \boldsymbol{\theta}^\top \mathbf{x} \right\|_F^2\end{aligned}$$

Observe that the term $\boldsymbol{\Sigma}$, whose entries (on the diagonal) $\sum_{i=1}^q \mu_i^2 \mathbf{M}_{i,j} = \frac{1}{q} \sum_{i=1}^q (\sqrt{q} \mu_i)^2 \mathbf{M}_{i,j}$ converge in probability to α as $q \rightarrow \infty$, captures all the effects of $\boldsymbol{\mu}$ and \mathbf{M} on the risk. Thus we can effectively replace $\boldsymbol{\Sigma}$ with $\alpha \mathbf{I}_p$

$$\mathbf{Risk} = \mathbb{E} \left\| \frac{\alpha}{\lambda} \mathbf{y}^\top \mathbf{F} \mathbf{W}\mathbf{x} - \frac{\alpha^2}{\lambda^2} \mathbf{y}^\top \mathbf{F}^\top \mathbf{F} \left(\frac{\alpha}{\lambda} \mathbf{F}^\top \mathbf{F} + \mathbf{I} \right)^{-1} \mathbf{F}^\top \mathbf{W}\mathbf{x} \right\|_F^2. \quad (3)$$

It remains to show that the expression of the risk is exactly the same as the risk in the setting of Section 3.1 with λ replaced by λ/α . Write down the risk in Section 3.1 (for convenience denote it by \mathbf{Risk}_0):

$$\begin{aligned}\mathbf{Risk}_0 &= \mathbb{E} \left\| \mathbf{y}^\top \mathbf{F}^\top (\mathbf{F} \mathbf{F}^\top + \lambda \mathbf{I})^{-1} \mathbf{W}\mathbf{x} - \boldsymbol{\theta}^\top \mathbf{x} \right\|_F^2 \\ &= \mathbb{E} \left\| \frac{1}{\lambda} \mathbf{y}^\top \mathbf{F} \mathbf{W}\mathbf{x} - \frac{1}{\lambda^2} \mathbf{y}^\top \mathbf{F}^\top \mathbf{F} \left(\frac{1}{\lambda} \mathbf{F}^\top \mathbf{F} + \mathbf{I} \right)^{-1} \mathbf{F}^\top \mathbf{W}\mathbf{x} \right\|_F^2.\end{aligned}\quad (4)$$

Equation 4 is obtained by applying Woodbury matrix identity to $(\mathbf{F} \mathbf{F}^\top + \lambda \mathbf{I})^{-1}$. It is easy to check that replacing λ in the RHS equation 4 with λ/α yields the RHS in equation 3.

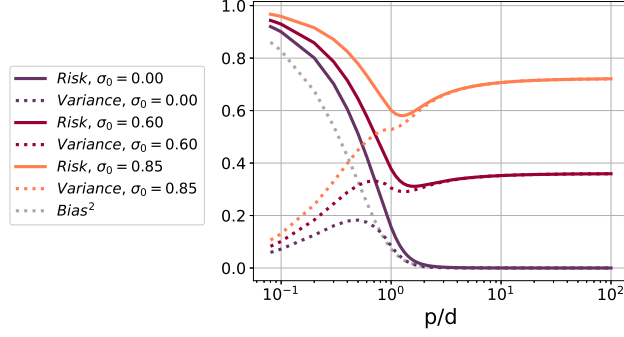


Figure 16: Risk, bias and variance given by expressions in section C.2 and Theorem 1.

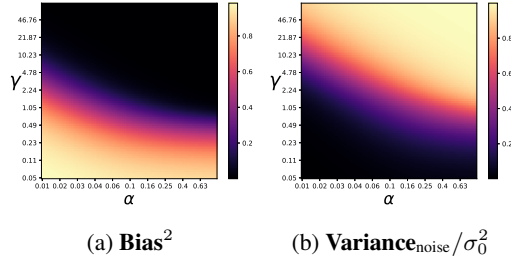


Figure 17: Expressions of Bias^2 and $\text{Variance}_{\text{noise}}/\sigma_0^2$ in Theorem 2

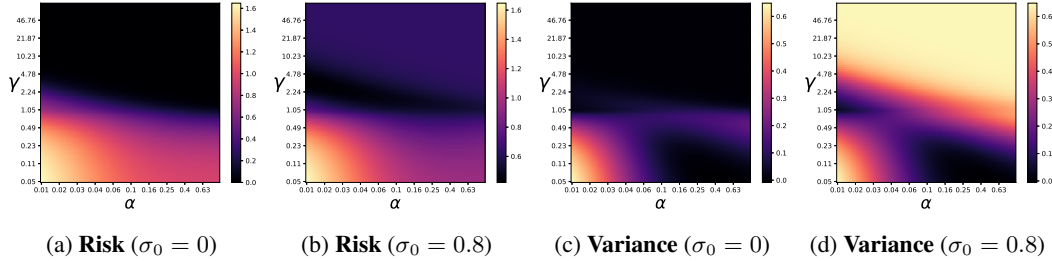


Figure 18: Expressions of the risk and variance under different noise levels with $\kappa = \gamma$. We let $\lambda_0 = 0.05$.

C.5 Variants of Theorem 2

In Theorem 2 we let μ 's entries be drawn from $\mathcal{N}(0, 1/q)$ so that q does not appear in the expression of the risk. Alternatively we can let μ 's entries be drawn from $\mathcal{N}(0, 1/d)$ and assume $q/d = \kappa$. Then the risk and its decomposition are dependent on γ, κ, α . Similar to the proof in C.4, we can show that in this case one just need to replace λ_0 in the setting of Theorem 1 with $\lambda_0/(\kappa\alpha)$ to get the expressions of risk. In Figures 18 and 19 we further let $\kappa = \gamma$ and generate the heatmaps.

C.6 Plots of Theoretical Expressions

Bias² and Risk in Section 3.1 In Figure 16 we plot **Risk**, **Bias²** and **Variance** based on expressions in section C.2 and Theorem 1. We see that **Bias²** is monotonic and **Risk** turns from monotonic to U-shaped due to the second ascent in variance as we increase noise.

Bias² and Variance_{noise}/sigma₀² in Section 3.2 In Figure 17 we plot the expressions of **Bias²** and **Variance_{noise}/sigma₀²** based on Theorem 2. **Bias²** monotonically decreases along both axes and **Variance_{noise}/sigma₀²** monotonically increases along both axes.

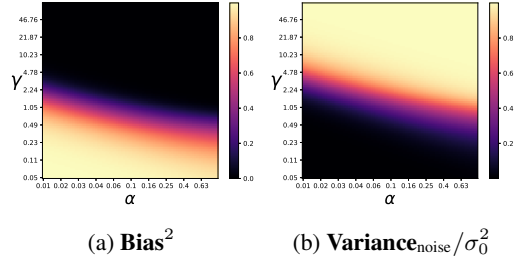


Figure 19: Expressions of **Bias**² and **Variance**_{noise}/ σ_0^2 with $\kappa = \gamma$.

Plots for section C.5 Figures 18 and 19 plot the expressions of **Risk** and all terms in its decomposition with $\kappa = \gamma$.